Fabrication and characterization of sub 100 nm period polymer gratings for photonics applications

K. Sangeeth and G. M. Hegde

We report on the fabrication of polymethylmethacrylate (PMMA) nanogratings on silicon (Si) and glass substrates using electron beam lithography technique. Various aspects of proximity corrections using Monte Carlo simulation have been discussed. The fabrication process parameters such as proximity gap of exposure, exposure dosage and developing conditions have been optimized for high-density PMMA nanogratings structure on Si and glass substrates. Electron beam exposure is adjusted in such a way that PMMA acts as a negative tone resist and at the same time resolution loss due to proximity effect is minimum. Both reflection and transmission-type, nanometre period gratings have been fabricated and their diffraction characteristics are evaluated.

Recent developments in advanced micro and nanofabrication techniques have enabled the fabrication of substrates that are able to recapitulate the structure and length scale of native topography on two-dimensional substrates. Dense and uniform features at nanoscale are extremely important in magnetic storage devices, sub-micron optical components, photo-detectors, etc. Fabrication of various nanotopographic geometries such as nanopillars, nanogratings, nanopits, etc. has been reported in the literature and their specific applications have also been demonstrated[1–6]. Among them, nanogratings are the more attractive because of their widespread applications in photonics and biotechnology. The diffraction gratings are typical passive optical elements for photonics applications such as communication (multiplexing, coupling, filtering), high-resolution encoders, spectroscopes, hologram elements and switching elements. Recently, there has been a lot of interest in nanograting structures since higher diffraction effects can be achieved from the higher aspect ratio structure for the multi-wavelength diffractive optical elements (DOEs). It has been reported that nanograting substrates can also be utilized as a tool to study complex cell functions such as adhesion, migration, cytoskeleton reorganization, cell polarization, and also to study contact guidance and migration *in vitro*[7]. Application of nanograting as force sensor for the characterization of neuron membrane mechanics is also reported[8]. There are a number of reported techniques for the fabrication of nanoscale gratings such as EUV[9], laser direct writing, focused ion beam (FIB)[10], synchrotron radiation lithography (SRL)[11], etc. However, there is enough scope for developing a standard and high throughput fabrication technique for such nanotopographic geometries.

Electron beam lithography (EBL) has been used extensively for prototyping devices with extremely small dimensions[12–14]. EBL is also used in mask-making for photolithography as well as X-ray lithography. New-generation E-beam systems use multiple electron beams[15] that basically increase the throughput of the process; however, the electron interaction with substrate material limits the dimensional features of the desired high-density nanostructures. Therefore, understanding of electron solid interaction is of extreme importance for the optimization of whole E-beam lithography process while fabricating densely packed structures such as nanometre period grating structures. In this paper we have optimized the E-beam lithography process for writing sub 100 nm period, high-density gratings on polymethylmethacrylate (PMMA) coated on silicon (Si) substrate. PMMA is used owing to its good mechanical and optical surface quality, minimal shrinkage and biocompatibility. Also, PMMA is an industrially widely known polymeric material in modern micro-nanotechnology. Proximity effect and energy density profile of the electron beam inside the PMMA coated on Si and Si/Au are evaluated using Monte Carlo simulation. Using the simulation results of optimized E-beam energy and dosage, grating structures were written on PMMA on Si, Si/Au and glass substrates. Both reflection and transmission nanogratings were fabricated and their diffraction characteristics have been evaluated.

Proximity correction simulation

Monte Carlo calculations are proved to be an appropriate method to simulate electron scattering in solid targets with application to electron emission and spectroscopy, electron probe microanalysis, X-ray mask writing and EBL[16–18]. EBL is capable of producing extremely small dimensions. But the scattering of energetic electron with resist material and the substrate results in the broadening of the beam, resulting in proximity effects. Proximity effect is due to the backscattered electrons from the substrate, which exposes the area surrounding the point of exposure. As the electron passes through resist layer (generally few hundreds of nanometres width), electrons undergo collisions with resist and give rise to secondary electrons, which are of few electron volts (eV) in energy. These secondary electrons are absorbed easily by the resist and along with forward scattering, this is a main reason for resist exposure. Electrons reaching the substrate undergo elastic scattering with the substrate and get reflected back to the resist through large angles. These electrons are again a reason for unwanted exposure of the resist. Proximity correction simulation is useful to decide the incident energy distribution depending on the electron–solid interaction such that the proximity effect is minimized. The electron energy density profile $f(r)$ can be expressed as[17,18]

$$f(r) = \frac{1}{1+\eta}\left\{\frac{1}{\pi\alpha^2}\exp\left(-\frac{r^2}{\alpha^2}\right) + \frac{1}{\pi\beta^2}\exp\left(-\frac{r^2}{\beta^2}\right)\right\}, \quad (1)$$

where η is the ratio between forward and backscattered energy, the term with α is a measure of forward scattering, the term with β is a measure of backscattering, and r is the distance from the point of incidence.

Beam energy and thickness of the resist are the two main parameters that define the energy density profile. When the beam energy is low (<10 kV), the forward scattering is high in the resist layer and backscattering is negligible for a thick resist layer. But for high beam energy, forward scattering is less but backscattering increases. One can tune the resist thickness so that the scattering in the resist is minimized. Also, with low atomic weight substrates, backscattering can be reduced. But in semiconductor industry, these are impractical since resist thickness and substrates are mostly fixed. Monte Carlo simulation of electrons with 30 kV energy hitting on 60 nm PMMA/bulk Si stack and 60 nm PMMA/50 nm Au/bulk Si stack was done using Casino[19,20] (Figure 1).

We used RaithNanoPEC software package for proximity correction. It simulates the scattering event based on Monte Carlo scheme for a given stack of materials. Also, it fractures the pattern into smaller elements and applies dose modification in such a way that effective dose and hence energy distribution are same throughout the pattern.

Fabrication and characterization

PMMA diffraction grating structures are fabricated on Si and glass substrates. The process steps are shown in Figure 2. The 80 nm thick PMMA was spin-coated on Si substrate at 6000 rpm and prebaked at 180°C for 10 min. We exposed this PMMA resist in a Raith E-LiNE direct EBL system at an accelerating potential of 30 kV. Exposure was done at 300 μC/cm^2. The negative tone of the required pattern was obtained in this lithography step. This sample was developed in MIBK : IPA solution (1 : 3) for 45 sec. This first exposure was also used to define the necessary alignment marks to allow the overlay exposure of the patterns. The sample was loaded again to the EBL system for a second exposure of the patterns with high dose. The second exposure dose was set in such a way that the dwell time of the beam in prepatterned regions was so high that the PMMA was cross-linked because of heating by the electron beam[21]. Generally doses more than 10 times the clearing dose will make PMMA cross-linked. The second exposure was done at 10 kV and the exposure dose was set to 5000 μC/cm^2. Sample was developed in acetone, since cross-linked PMMA does not dissolve in acetone whereas the other unwanted portions will be removed in acetone. In order to enhance the reflectivity of the grating, we repeated the same fabrication process with 50 nm Au metal layer between PMMA and bulk Si substrate, using optimized energy dose from the proximity simulation results. The same process steps were extended to write the PMMA nanostructure on glass substrate.

Proximity calculations were done only in the case of the first lithography. This is the step where finer patterns are defined and hence proximity effects should be taken into account. This exposure was done at the highest possible beam energy since it reduces forward scattering of electron beam in the resist. The aim of second exposure was just to harden the PMMA and hence no proximity calculations were done. The cross-linked PMMA is extremely stable towards normal solvents. In this case exposure was done at comparatively low energies so that electron beam-induced heating takes place mainly in the resist and top layers of Si substrate which increases the chance of cross-linking. High density (≈14,700 lines/mm) rectangular groove, 68 nm period PMMA grating patterns were fabricated on Si and 50 nm Au/Si substrate. Following the same EBL process, high-density (≈14,000 lines/mm) PMMA transmission nanograting was fabricated on 0.5 mm thick glass substrate. Figure 3 shows the SEM images (30 K × Mag.) of the PMMA nanogratings fabricated on different substrates. The SEM images clearly show the difference in the grating pitch and critical dimension between two different substrates, even though the exposure was done under the same conditions. It is

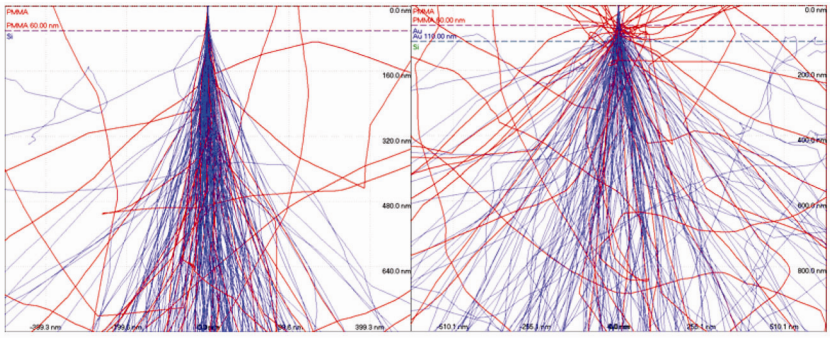

Figure 1. Monte Carlo simulation of 30 kV electrons scattering in the material stack – (Left) On 60 nm thick polymethylmethacrylate (PMMA)/bulk Si and (Right) on 60 nm PMMA/50 nm Au/bulk Si. *X*-direction; Radial distance (nm) from the centre of the beam spot. *Y*-direction; Penetration depth (nm) into the material.

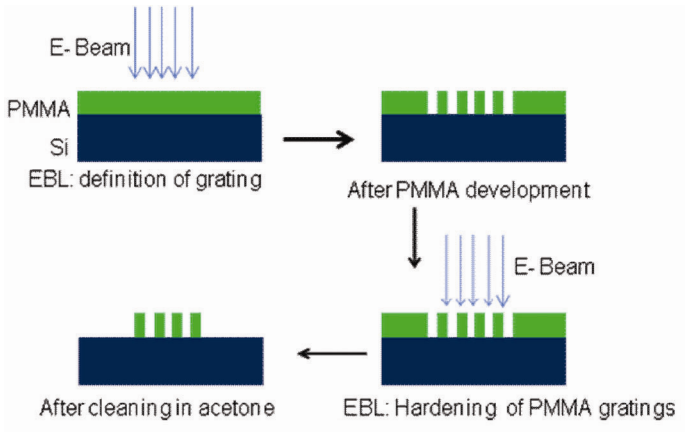

Figure 2. Illustration of the fabrication process.

clear from the SEM images that in case of PMMA on Si and glass substrates (Figure 3 *a* and *c*), the line edges are sharp and there is no resist swelling along the line after processing. However, on gold-coated Si (Figure 3 *b*), the grating lines are nonuniform and there is discontinuity in the lines with distorted edges. Also, the gold film was clustered to form island structures leading to poor reflectivity. Furthermore, we have characterized the surface morphologies using AFM, as shown in Figure 4 *a*. The measured depth of the grooves is about 15 nm on average, as shown in Figure 4 *b*. This further confirms nearly the rectangular groove of PMMA gratings with pitch 69 nm and depth 15 nm.

Figure 5 *a* and *b* shows the experimental set-up used for studying the diffraction characteristics of the PMMA nanogratings. A linearly polarized He–Ne laser beam (632.8 nm) was used for the study. The position of the grating was carefully adjusted so that laser spot falls on 1 mm grating area. The diffraction pattern was projected onto a screen kept at a known distance. Figure 5 *c* and *d* shows the images of diffraction patterns of 632.8 nm laser beam generated from PMMA reflection and transmission gratings. From the figure we can see more than 10 orders of diffraction in the case of PMMA nanogratings written on Si and glass substrates. However, in the case of PMMA grating written on gold-coated Si substrate, no clear diffraction pattern was observed.

One of the important characteristics of diffraction gratings to be analysed is their resolving power. The theoretical resolving power of a planar diffraction grating is given in optics textbooks[22] as

$$R = mN, \tag{2}$$

where m is the diffraction order and N is the total number of grooves illuminated on the surface of the grating. In our case, since the grating area is 1 mm^2, the entire grating area is illuminated with the laser beam. Hence the maximum attainable resolving power is given as

$$R_{\max} = \frac{2W}{\lambda}, \tag{3}$$

regardless of the order m or number of grooves N under illumination[22], where W is width of the grating and λ is wavelength of the light. Using the above relation, the calculated resolving power of our PMMA nanograting is of the order 3.16×10^3 at a wavelength of 632 nm, for both reflection and transmission configurations.

Another important property is the diffraction efficiency. For a given wavelength, the distribution of power (diffraction efficiency) diffracted by a grating into various spectral orders depends on many parameters, such as power and polarization of the incident light, angles of incidence and diffraction, refractive index of the grating materials and groove spacing and shape. A complete analysis of grating efficiency requires the vector formulation of electromagnetic theory applied to different grating surfaces, which has been well studied over the past few decades. It has also been reported that diffraction gratings with rectangular grooves normally have higher diffraction efficiency[23]. As a thumb rule we estimated diffraction efficiency of PMMA nanograting by measuring diffracted laser power through a pinhole as shown in Figure 5 *a* and *b*. Since the grating area is very small (1 mm^2) and the laser beam diameter is 2 mm and power 3 mW, we have considered the power density spread only in 1 mm^2 area of the grating as the incident

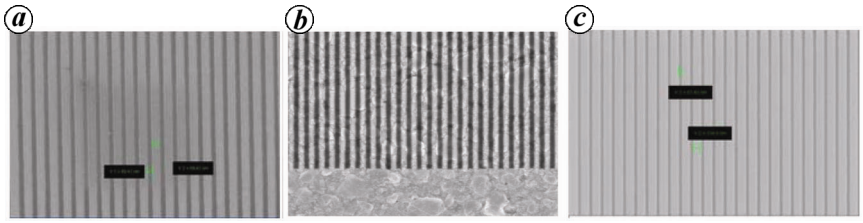

Figure 3. SEM images of cross-linked PMMA pattern on (***a***) Si, (***b***) 50 nm Au/Si and (***c***) glass.

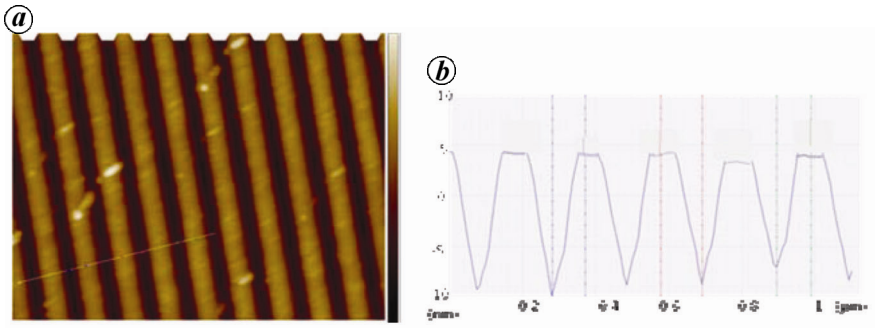

Figure 4. ***a***, A 3D view of the AFM image. ***b***, Measured step height of the PMMA nanogratings on Si.

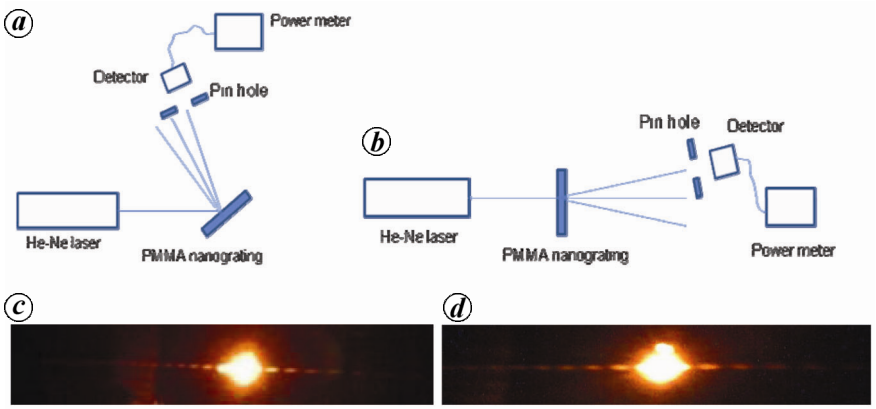

Figure 5 ***a***, ***b***. Experimental set-up for studying the diffraction properties: ***a***, reflection grating; ***b***, transmission grating and diffraction pattern of 632.8 nm wavelength obtained from PMMA; ***c***, ***d***, Diffraction patterns generated using (***c***) reflection grating and (***d***) transmission grating.

power in our calculation. Also because of this the first-order diffraction was almost overlapping with the zeroth-order, making it difficult to measure the diffracted power. Hence we have considered the second and higher orders for our calculation. To quantify the relative zeroth and second-order diffraction efficiency of PMMA nanograting, the following expression was used[24]

$$\eta = \frac{T_{0,2}}{T_{\text{total}}}, \quad (4)$$

where $T_{0,2}$ denotes the reflected power of the zeroth and the second-order beams respectively, and T_{total} is the total reflected laser power including all orders. In our experiment we are able to measure the diffracted power up to tenth order. For the PMMA nanogratings (reflection and transmission) we have fabricated, the calculated second-order diffraction efficiency, $\eta \approx 15\%$. Thus we have proposed a simple EBL process to fabricate large-area polymer (PMMA)-based nanogratings on Si and glass substrates and the process can be extended to fabricate other PMMA-based nano-optical components.

Conclusion

We have carried out proximity correction using Monte Carlo simulation for the fabrication of polymer (PMMA) nanograting structure on Si, gold-coated Si and glass substrates using EBL. The results were used to optimize the input dose to the primary GDSII file, so that exposure dose is adjusted to get resultant uniform dose throughout the large-area dense nanostructure. Using these results PMMA-based 68 nm period gratings were fabricated on Si, Au/Si and glass substrates. With double exposure PMMA was made to cross-link, thus enhancing the structural stability of the device without losing its high-resolution property. Diffraction properties of the polymer nanogratings have been evaluated to verify the performance of fabricated devices. Grating resolving power of the order 3.16×10^3 and first-order diffraction efficiency of about 15% have been achieved for the PMMA grating fabricated on Si and glass. Gratings with PMMA coated on thin gold layer on Si were also fabricated; however, the observed diffraction properties are of poor quality. These polymer nanogratings may find widespread applications not only in nanophotonics but also in biology, as these nanostructures can be used as a tool to study complex cell functions.

1. Dial, O., Cheng, C. C. and Scherer, J. A., *Vac. Sci. Technol. B*, 1998, **16**, 3887–3392.
2. Chou, S. Y., Krauss, P. R. and Renstrom, P. J., *Appl. Phys. Lett.*, 1995, **67**, 3114–3116.
3. Rafiq, M. A., Mizuta, H., Shigeyasu Uno, Z. A. K. and Durrani, Z. A. K., *Microelectron. Eng.*, 2007, **84**, 1515–1518.
4. Gopal, A. *et al.*, *Biomed. Microdevices*, 2008, **10**(5), 611–622.
5. Koster, R., Hovel, H., Bruchhaus, L., Bauerdick, S., Thiel, J. and Jede, R., *J. Appl. Phys.*, 2007, **101**, 044301–044306.
6. Hsu, C. M., Stephen, T. C., Mary, X. T. and Yi Cui, *Appl. Phys. Lett.*, 2008, **93**, 133109.
7. Bettinger, C. J., Langer, R. and Borenstein, J. T., *Angew. Chem., Int. Ed. Engl.*, 2009, **48**(30), 5406–5415.
8. Gopal, A. *et al.*, *IEEE Proc. Solid-State Sensors, Actuators Microsyst., Transducers*, 2007, 1239–1242.
9. Ekinci, Y., Solak, H. H., Padeste, C., Gobrecht, J., Stoykovich, M. P. and Nealey, P. F., *Microelectron. Eng.*, 2007, **84**, 700–704.
10. Yao, B. Y., Hu Luo, Feng, L. S., Zhou, Z., Wang, R. M. and Chi, Y. Y., *Key Eng. Mater.*, 2011, **83**, 66–69.
11. Kato, F., Fujinawa, S., Li, Y. and Sugiyama, S., *Microsyst. Technol.*, 2007, **13**, 221–225.
12. Schmidt, M. S., Hübner, J. and Boisen, A., *Adv. Mater.*, 2012, **24**, OP11–OP18.
13. Zhang, D. G., Yuan, X. C. and Teng, J., *Appl. Phys. Lett.*, 2010, **97**, 231117–231119.
14. Lei, X., Wu, L., Deshpande, P., Yu, Z., Wu, W., Ge, H. and Chou, S. Y., *Nanotechnology*, 2003, **14**, 786–790.
15. Chang, T. H. P., Mankos, M., Lee, K. Y. and Mura, L. P., *Microelectron. Eng.*, 2001, **57–58**, 117–135.
16. Seo, E., Choi, B. K. and Kim, O., *Microelectron. Eng.*, 2000, **53**, 305–308.
17. http://nanolithography.gatech.edu/proximity.htm
18. Aya, S., Kise, K., Yabe, H. and Marumoto, K., *Jpn. J. Appl. Phys.*, 1996, **35**, 1929–1936.
19. Owen, G., *J. Vac. Sci. Technol. B*, 1990, **8**, 1889–1894.
20. Drouin, D., Couture, A. R., Joly, D., Tastet, X., Aimez, V. and Gauvin, R., *CASINO V2.42*, 2007, **29**, 92–101.
21. Zailer, I., Frost, J. E. F., Chabasseur-Molyneux, V., Ford, C. J. B. and Pepper, M., *Semicond. Sci. Technol.*, 1996, **11**, 1235–1238.
22. Hecht, E., *Optics,* Addison-Wesley, 1987, pp. 424–430.
23. Haidner, H. *et al.*, *Infrared Phys.*, 1993, **34**, 467–475.
24. Ren, H., Fan, Y. H. and Wu, S. T., *Appl. Phys. Lett.*, 2003, **82**, 3168–3170.
25. Liu, Y. J., Loh, W. W., Leong Eunice, S. P., Kustandi, T. S., Sun, X. W. and Teng, J. H., *Nanotechnology*, 2012, **23**, 465302–465307.

ACKNOWLEDGEMENT. We thank the Centre for Nano Science and Engineering, Indian Institute of Science, Bangalore for providing the necessary facilities.

Received 15 March 2014; revised accepted 9 August 2014

K. Sangeeth and G. M. Hegde are in the Centre for Nano Science and Engineering, Indian Institute of Science, Bangalore 560 012, India.*
**e-mail: nanogopal@cense.iisc.ernet.in*